Journal of Alloys and Compounds 509 (2011) 6423–6426

Contents lists available at ScienceDirect

Journal of Alloys and Compounds

journal homepage: www.elsevier.com/locate/jallcom

Effects of silver addition on microstructure and electrical properties of barium titanate ceramics

Pengrong Ren, Huiqing Fan*, Xin Wang, Jin Shi

State Key Laboratory of Solidification Processing, School of Materials Science and Engineering, Northwestern Polytechnical University, Xi'an 710072, China

ARTICLE INFO

Article history:
Received 5 January 2011
Received in revised form 8 March 2011
Accepted 13 March 2011
Available online 21 March 2011

Keywords:
Composite materials
Microstructure
Dielectric response

ABSTRACT

Barium titanate–silver composites were prepared by using a solid state reaction process with silver contents ranging from 0 mol% to 20 mol%. XRD results and Raman spectra indicated that there was no phase other than $BaTiO_3$ and Ag in the ceramics and tetragonality of barium titanate reduced with increasing Ag content. SEM images illustrated that Ag influenced densification and microstructure of $BaTiO_3$ ceramics. Besides, addition of Ag led to increase in dielectric permittivity and broadening of ferroelectric–paraelectric phase transition peak. Also addition of Ag had effects on dielectric loss and dc conductivity. Dielectric and conductivity properties as a function of Ag volume fraction were explained by the percolation theory.

1. Introduction

Barium titanate ($BaTiO_3$) has become one of the most important dielectric materials in electronics industry for last decades. Due to its high dielectric constant, it has been widely used in multilayer ceramic capacitor (MLCC) materials [1,2]. However, with the development of MLCC toward high-capacity, miniaturization and thin-layer, we must further enhance dielectric constant and improve temperature stability of $BaTiO_3$ ceramics [3].

Recently, ceramic–metal composites have been studied in the context of high dielectric constant [4]. The corresponding percolation threshold theory has been established and it was predicted that ceramic–metal composites could obtain giant dielectric permittivity when the volume fraction of metal close to the percolation limit [5,6]. And several experiments have confirmed a modest increase in dielectric permittivity of ceramic–metal composites [7–10]. Among various metallic powders used in ceramic–metal composites, Pt and Pd are too expensive and Al, Cu and Ni have the problem of oxidization while sintering at higher temperatures [11]. Hence silver is thought to be reasonable candidate used in ceramic–metal composites. Chen et al. [12] studied the effect of silver on the sintering and grain-growth behavior of barium titanate and determined the solubility of silver in barium titanate. Chen et al. [13] and Halder et al. [14] respectively investigated effects of silver addition on dielectric properties of barium titanate-based X7R and Z5U ceramics. However, according to the percolation theory, when the volume fraction of metal close to the percolation limit, conductivity of composites also increases significantly, leading to weakening of resistivity property, which is not favorable for MLCC materials. Previous studies less simultaneously considered silver addition generated effects on both dielectric and conductivity properties of barium titanate ceramics.

In this paper, effects of different silver contents (0.0–20.0 mol%) on the phase constitution, microstructure, dielectric and conductivity properties of barium titanate ceramics were investigated.

2. Experimental procedure

Barium titanate composites with 0, 4, 6, 8, 10, 15, 20 mol% silver (respectively labeled with BTA0, BTA4, BTA6, BTA8, BTA10, BTA15, BTA20) were prepared by the conventional solid state ceramic route. Analytical purity $BaCO_3$, TiO_2 and Ag_2O were used as the starting materials. Stoichiometric amounts of the powder samples were mixed and ball milled using zirconia balls in ethanol medium for 6 h. The resultant slurry was then dried, pressed into cylindrical samples and then calcinated at 1100 °C for 2 h. The calcinated cylindrical samples were then crushed and ball milled for 12 h. The final powders were compacted into pellets by cold isostatic pressing at 200 MPa for 90 s. Silver free $BaTiO_3$ were sintered at 1250 °C for 4 h and other pellets were sintered at 1230 °C for 2 h. During sintering, all the pellets were covered in Al_2O_3 crucibles.

Because very small silver spheres condensed on the surface of the disks during the cooling process from the silver gas evaporated at temperature higher than 1000 °C, sintered pellets were polished and then did some measurements. Phase structure was investigated by using X-ray diffraction (XRD) (D/Max2550VB+/PC, Rigaku, Tokyo, Japan) with Cu Kα radiation ($\lambda = 0.15406$ nm) over 2θ range of 20–80°. Diffraction spectra was collected at a scan rate of 2.5°/min. Raman spectra were measured on pellets at 100–1000 cm^{-1} by Raman Microscope (inVia, Renishaw, London, England). The spectral excitation was provided by an Ar^+ laser, using the 514.5 nm line and with proper power density on the sample surface. Morphology of natural surface of sintered pellets was examined by using an optical microscopy (OM) (OLYMPUS-PMG3, Olympus. Co., Tokyo, Japan) and a field-emission scanning electron microscopy (FE-SEM) (JEOL-6700F, Japan Electron Co., Tokyo, Japan) operated

* Corresponding author. Tel.: +86 29 88494463; fax: +86 29 88492642.
E-mail address: hqfan3@163.com (H. Fan).

0925-8388/$ – see front matter © 2011 Elsevier B.V. All rights reserved.
doi:10.1016/j.jallcom.2011.03.077

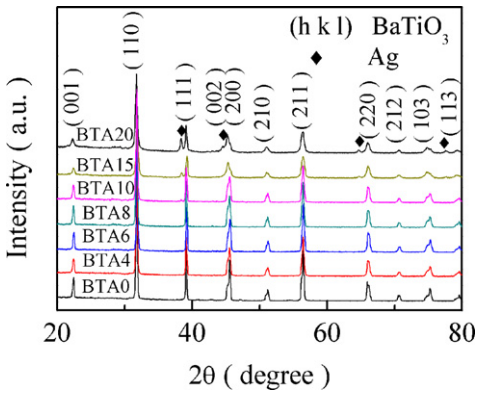

Fig. 1. XRD patterns of BTA0–BTA20.

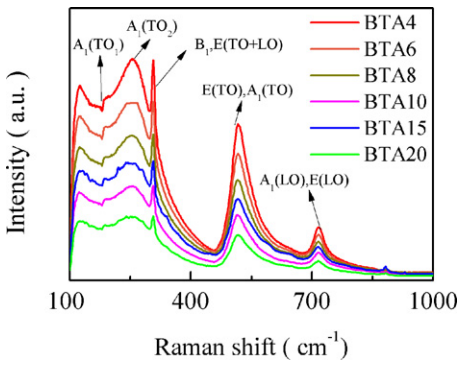

Fig. 2. Raman spectra of BTA4–BTA20.

at 20 kV. Silver electrodes with appropriate configurations were coated on both polished surfaces and fired at 550 °C for 30 min to form a metal–insulator–metal (MIM) capacitor for electrical test. Weak-field dielectric response at a signal level of 500 mV/mm was measured by using a precision impedance analyzer (4294A, Agilent, CA, USA) associated with temperature controller (TP94, Linkam, Surrey, UK) from room temperature to 200 °C at a heating rate of 2 °C/min. A high resistance meter (4339B, Agilent, CA, USA) was employed to measure the dc conduction from 200 °C to room temperature at the cooling rate of 2 °C/min.

3. Results and discussion

XRD patterns of BTA0–BTA20 are shown in Fig. 1. XRD analysis indicates that no phases other than $BaTiO_3$ and silver are present in the ceramics. It suggests that no reaction took place between $BaTiO_3$ and silver during calcinations and sintering. Thermodynamic studies have suggested that silver is more stable than Ag_2O at temperatures of >189.8 °C in air [15]. Therefore, any Ag_2O that is present decomposes to metallic silver during the calcination heating-up stage. In the cooling stage from the calcination temperature, the amount of Ag_2O that is formed is very low since the formation of Ag_2O is a very slow process at low temperature [12]. So no Ag_2O is observed in the XRD spectrum. For BTA4, BTA6, BTA8, the diffraction peak of Ag does not appear. According to the study of Shih and Tuan [16], the solubility of silver in the $BaTiO_3$ was as low as 450 ppm, after cofiring at 1290 °C for 2 h in air, which excludes the possibility that Ag element entirely solutes in the $BaTiO_3$ crystal. It can be explained that Ag gas evaporated during calcinations and sintering, so low concentration of Ag in the composites is not detected by XRD. We calculated the real contents of silver in the samples according to diffraction peaks of barium titanate and silver in XRD spectrums using MDI Jade 5.0 programme. The contents of silver in the BTA20 and BTA15 samples are respectively about 14.1 mol% and 10.5 mol%. Besides, it can be seen that for pure $BaTiO_3$, reflection peaks of (0 0 2) and (2 0 0) obviously split. With increasing Ag content, the split is weakened, suggesting that tetragonality of barium titanate decreases, which can be further verified by Raman spectra.

Fig. 2 shows Raman spectra of BTA4–BTA20. As shown in Fig. 2, the modes located at about 180, 307 and 720 cm^{-1} are related to tetragonal phase [17] and the modes at about 256 and 518 cm^{-1} are related to order–disorder phase [18]. With increasing Ag content, Raman intensity of $BaTiO_3$/Ag composites gradually decreases and spectra peaks become weaker and broader, indicative of tetragonal symmetry reducing and some structural reordering taking place.

Fig. 3(a–g) displays SEM images of natural surface of BTA0–BTA20. For BTA0, it shows dense microstructure and the average grain size is about 0.8 μm. However addition of Ag changes the sintering activity. As shown in Fig. 3(b–f), grains similar to spheres in shape loosely neck together and pores appear in the ceramics. Significant numbers of abnormal grains are not observed in the samples fabricated in this study. The wettability of silver on $BaTiO_3$ substrate was studied by Wang et al. [19]. The results showed that the contact angle between silver liquid and $BaTiO_3$ substrate is still 128° at 1150 °C, which means that the wettability of silver on $BaTiO_3$ is very weak. So during sintering process, liquid silver obstructs the diffusion between $BaTiO_3$ grains, and as a result inhibits the densification process. For BAT20, as seen in Fig. 3(g), large amount of silver migration leads to the so-called Ag-tree formation [20]. Fig. 3(h) illustrates optical photos of polished surface of BTA15. Silver particles agglomerate and show "island" distribution in the polished surface of sample.

Fig. 4 shows temperature dependence of dielectric permittivity (ε') at 1 kHz for BTA0–BTA20. As can be seen, addition of Ag obviously leads to the increase in dielectric permittivity and the ferroelectric–paraelectric phase transition peak is broadened, but the Curie temperature does not changed. The results are in agreement with previous XRD and Raman analysis that tetragonality of barium titanate decreases with increasing Ag content and Ag does not enter into the crystal lattice of $BaTiO_3$.

The relative permittivity of ceramic–mental composites can be predicted by using the Maxwell's equation [21] as

$$\varepsilon(f) = \varepsilon_m \left[\frac{1+2f}{1-f}\right] \quad (1)$$

where ε_m is the relative permittivity of the matrix, f is metal volume fraction. According to this model, the increase in dielectric permittivity can be understood as the conducting particle apparently shortening the electrode distance, thereby increasing the effective electric field in the dielectric phase [14]. The relative permittivity can also be estimated by using a percolation law [22] as

$$\varepsilon(f) = \frac{\varepsilon_m}{|f_c - f|^q} \quad (2)$$

where f_c is the percolation threshold, q is a constant. The percolation theory predicts a dramatic increase in relative permittivity as the volume fraction is approaching its percolation threshold.

Fig. 5 shows experimental measured values of dielectric permittivity and predicted values from Maxwell's equation and percolation law, using $f_c = 0.16$ (the theoretical value for a random composite) and $q = 3.0$. The results indicate that dielectric permittivity as a function of Ag volume fraction in our study is more in agreement with percolation law. The slight deviation from percolation law of BTA6 and BTA8 might be attributed to the decrease of density in ceramics. For BAT20, the dramatic reduce of dielectric permittivity is due to the formation of Ag-tree in the ceramics.

Figs. 6 and 7 show dielectric loss and dc conductivity as a function of temperature for BTA0–BTA20. It can be seen that both dielectric loss and dc conductivity decrease after addition of Ag for BTA4–BTA10, which might be associated with the reduction of density. For BAT15, it shows low dielectric loss, however, the

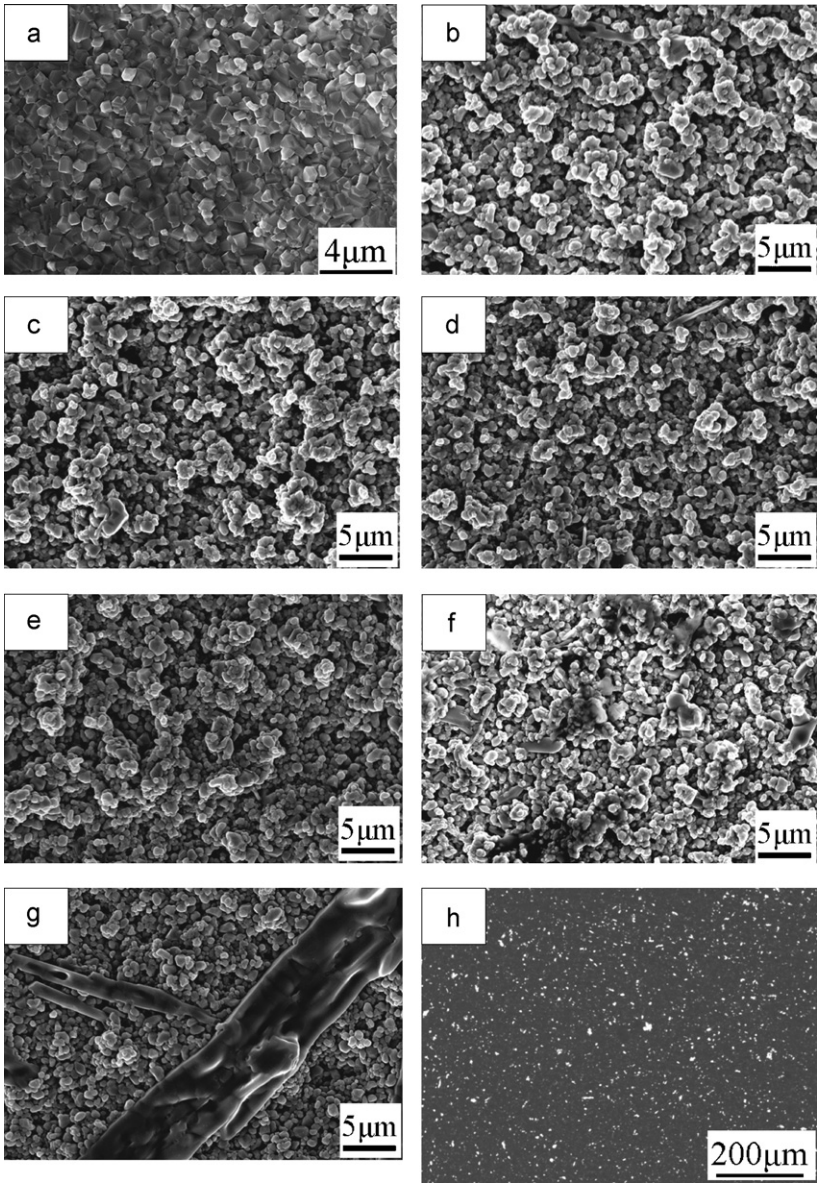

Fig. 3. SEM images of natural surface of BTA0–BTA20: (a) BTA0, (b) BTA4, (c) BTA6, (d) BTA8, (e) BTA10, (f) BTA15 and (g) BTA20; (h) optical photos of polished surface of BTA15.

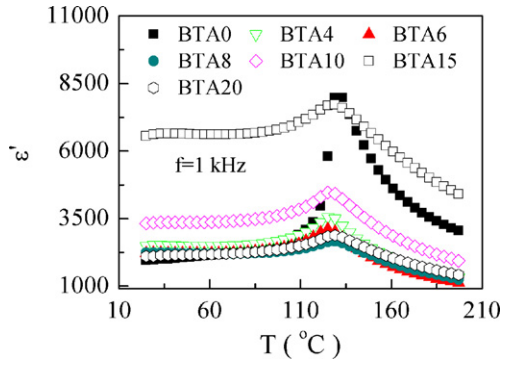

Fig. 4. Temperature dependence of dielectric permittivity (ε') at 1 kHz for BTA0–BTA20.

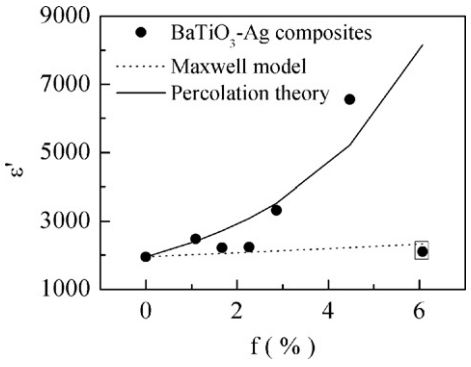

Fig. 5. Experimental measured values of dielectric permittivity and predicted values from Maxwell's equation and percolation law.

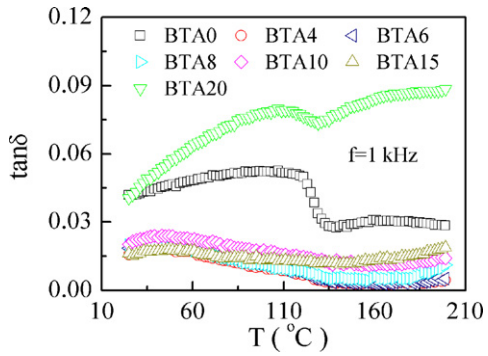

Fig. 6. Dielectric loss and dc conductivity as a function of temperature for BTA0–BTA20.

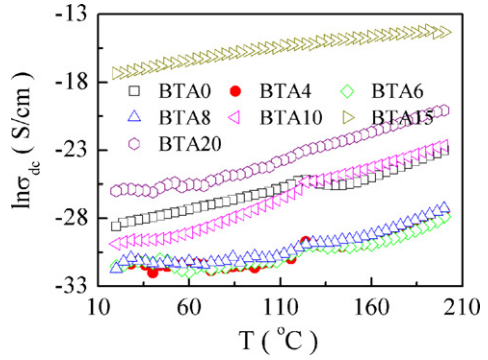

Fig. 7. dc conductivity as a function of temperature for BTA0–BTA20.

dc conductivity significantly increases several order of magnitude, which is not favorable for its application in MLCC. The increase in dielectric loss of BAT20 is also due to formation of Ag-tree in the ceramics.

4. Conclusions

Barium titanate composites with 0, 4, 6, 8, 10, 15, 20 mol% silver were prepared by the conventional solid state ceramic route. Silver did not react with $BaTiO_3$ during sintering, while it influenced densification and microstructure of $BaTiO_3$ ceramics. Spherical $BaTiO_3$ grains necked together and silver particles show island distribution in the ceramics. All these factors, such as density, microstructure and percolation threshold effects, had effects on dielectric and conductivity properties of barium titanate–silver composites. Barium titanate composites with 15 mol% Ag showed maximum dielectric permittivity, but it was accompanied by a significant increase in dc conductivity. Addition low concentrations of Ag (<10 mol%) in $BaTiO_3$ ceramics led to increase in dielectric permittivity, improvement of temperature stability and decrease in dielectric loss and dc conductivity, so it can be a candidate for application in MLCC materials.

Acknowledgements

This work was supported by the National Nature Science Foundation (50672075), the NCET and 111 Program (B08040) of MOE, Xi'an Science and Technology Foundation (XA-AM-200905, XA-AM-200906), the Fundamental Research Foundation (NPU-FFR-200703), the SKLSP Research Fund (40-QZ-2009) and Doctorate Foundation of NPU.

References

[1] H. Kishi, Y. Mizuno, H. Chazono, Jpn. J. Appl. Phys. 42 (2003) 1–15.
[2] S. Guillemet-Fritsch, Z. Valdez-Nava, C. Tenailleau, T. Lebey, B. Durand, J.Y. Chane-Ching, Adv. Mater. 20 (2008) 551–555.
[3] P. Yu, B. Cui, Z. Chang, Mater. Res. Bull. 44 (2009) 893–897.
[4] C. Pecharroman, F. Esteban-Betegón, J.F. Bartolome, S. López-Esteban, J.S. Moya, Adv. Mater. 13 (2001) 1541–1544.
[5] C.W. Nan, Prog. Mater. Sci. 37 (1993) 1–116.
[6] D.M. Grannan, J.C. Garland, D.B. Tanner, Phys. Rev. Lett. 46 (1981) 375–378.
[7] Y. Bai, Z.Y. Cheng, V. Bharti, H.S. Xu, Q.M. Zhang, Appl. Phys. Lett. 76 (2000) 3804.
[8] H.J. Hawang, M. Yasunoka, M. Sando, M. Toriyama, K. Niihara, J. Am. Ceram. Soc. 80 (1997) 791–793.
[9] D.J. Lewis, D. Gupta, M.R. Notis, Y. Imanaka, J. Am. Ceram. Soc. 79 (1996) 261–265.
[10] P.E. Sánchez-Jiménez, L.A. Pérez-Maqueda, M.J. Diánez, A. Perejón, J.M. Criado, Compos. Struct. 92 (2010) 2236–2240.
[11] S. George, M.T. Sebastian, Compos. Sci. Technol. 68 (2008) 2461–2467.
[12] C.Y. Chen, W.H. Tuan, J. Am. Ceram. Soc. 83 (2000) 2988–2992.
[13] R. Chen, X. Wang, Z. Gui, L. Li, J. Am. Ceram. Soc. 86 (2003) 1022–1024.
[14] N. Halder, A.D. Sharma, S.K. Khan, A. Sen, H.S. Maiti, Mater. Res. Bull. 34 (1999) 545–550.
[15] J. Assal, B. Hallstedt, L.J. Gauckler, J. Am. Ceram. Soc. 80 (1997) 3054–3060.
[16] S.J. Shih, W.H. Tuan, J. Am. Ceram. Soc. 87 (2004) 401–407.
[17] Z.H. Yao, H.X. Liu, Y. Liu, Z.H. Wu, Z.Y. Shen, Y. Liu, M.H. Cao, Mater. Chem. Phys. 109 (2008) 475–481.
[18] R. Naik, J.J. Nazarko, C.S. Flattery, U.D. Venkateswaran, V.M. Naik, M.S. Mohammed, et al., Phys. Rev. B 61 (2000) 11367–11372.
[19] S.F. Wang, T.C.K. Yang, S.C. Lee, J. Mater. Sci. 36 (2001) 825–829.
[20] J.M. Hubert, Ceramic Dielectrics and Capacitors, Gordon and Beech, New York, 1985.
[21] P. Chýlek, V. Srivastava, Phys. Rev. B 30 (1984) 1008–1009.
[22] C. Pecharromµn, J.S. Moya, Adv. Mater. 12 (2000) 294–297.